nature microbiology

Article

https://doi.org/10.1038/s41564-023-01593-7

Ammonia-oxidizing bacteria and archaea exhibit differential nitrogen source preferences

Received: 25 July 2023

Accepted: 15 December 2023

Published online: 31 January 2024

Check for updates

Wei Qin[1,2,12] ✉, Stephany P. Wei[2,12], Yue Zheng[3,12], Eunkyung Choi[4,12], Xiangpeng Li[1], Juliet Johnston[5], Xianhui Wan[6], Britt Abrahamson[2], Zachary Flinkstrom[2], Baozhan Wang[7], Hanyan Li[1], Lei Hou[1,3], Qing Tao[1], Wyatt W. Chlouber[1], Xin Sun[8], Michael Wells[1], Long Ngo[1], Kristopher A. Hunt[2], Hidetoshi Urakawa[9], Xuanyu Tao[1], Dongyu Wang[1], Xiaoyuan Yan[10], Dazhi Wang[3], Chongle Pan[1], Peter K. Weber[5], Jiandong Jiang[7], Jizhong Zhou[1], Yao Zhang[11], David A. Stahl[2], Bess B. Ward[6], Xavier Mayali[5], Willm Martens-Habbena[4] ✉ & Mari-Karoliina H. Winkler[2] ✉

Ammonia-oxidizing microorganisms (AOM) contribute to one of the largest nitrogen fluxes in the global nitrogen budget. Four distinct lineages of AOM: ammonia-oxidizing archaea (AOA), beta- and gamma-proteobacterial ammonia-oxidizing bacteria (β-AOB and γ-AOB) and complete ammonia oxidizers (comammox), are thought to compete for ammonia as their primary nitrogen substrate. In addition, many AOM species can utilize urea as an alternative energy and nitrogen source through hydrolysis to ammonia. How the coordination of ammonia and urea metabolism in AOM influences their ecology remains poorly understood. Here we use stable isotope tracing, kinetics and transcriptomics experiments to show that representatives of the AOM lineages employ distinct regulatory strategies for ammonia or urea utilization, thereby minimizing direct substrate competition. The tested AOA and comammox species preferentially used ammonia over urea, while β-AOB favoured urea utilization, repressed ammonia transport in the presence of urea and showed higher affinity for urea than for ammonia. Characterized γ-AOB co-utilized both substrates. These results reveal contrasting niche adaptation and coexistence patterns among the major AOM lineages.

Ammonia-oxidizing microorganisms (AOM) account for the oxidation of ~2,330 TgN yr^{-1}, representing one of the largest nitrogen fluxes in the global nitrogen budget[1]. Ammonia-oxidizing bacteria and archaea (AOB, AOA) oxidize ammonia (hereafter considered as total ammonia, $NH_3 + NH_4^+$) to nitrite[2,3], which is then oxidized to nitrate by nitrite-oxidizing bacteria (NOB), comprising the two-step process of nitrification. Recently, complete ammonia oxidizers (comammox), capable of oxidizing ammonia to nitrate, were discovered within the NOB genus *Nitrospira*[4,5]. Given that all AOM use ammonia as energy and nitrogen (N) sources for growth, their specific affinity for ammonia has been considered the main determinant of their competition and niche partitioning[6–8]. However, fundamental questions remain about

A full list of affiliations appears at the end of the paper. ✉e-mail: weiqin@ou.edu; w.martenshabbena@ufl.edu; mwinkler@uw.edu

the biochemical and biophysical controls of their specific affinities for ammonia[9,10]. Although different lineages of AOM are thought to compete for their primary N substrate, ammonia, they often grow concomitantly in soil, freshwater, estuarine and subsurface ecosystems, raising the question of other adaptative strategies that allow for their co-occurrence.

Microorganisms adapt to changing resource availability by either utilizing multiple substrates simultaneously or preferentially using those that support optimal growth with least investment in enzyme inventory, the latter exemplified by the glucose–lactose diauxie in *Escherichia coli*[11]. Most studies have focused on how microorganisms metabolize carbon (C) mixtures[12] or mixed N sources for anabolism[13,14]. Less is known about selection of alternative N substrates for catabolic energy conversion, a capacity unique to nitrifying microorganisms[1]. For example, an adaptive trait of many AOM species is the capacity to utilize urea as an energy and N source through hydrolysis to ammonia[4,15–20].

Urea is an important and widely available organic nitrogen compound in soil and aquatic environments, released as nitrogenous waste from both eukaryotes and prokaryotes and subsequently hydrolysed by ureolytic microorganisms[21,22]. Urea-based fertilizers are a mainstay in modern agriculture, and the intensive use of urea in fertilizers has greatly increased urea export to surrounding freshwater and coastal ecosystems. Since the urease enzyme does not require a high-energy cofactor, such as ATP[23], recent studies in marine systems suggested that ammonia and urea may be co-utilized for energy and N requirements[24]. However, utilization or even co-utilization of urea would require an investment in the synthesis of the urea transporter, urease and accessory proteins—a substantial cost for autotrophic AOM using the low energy-yielding ammonia oxidation process. Thus, there is a compelling need for better mechanistic understanding of urea utilization by ammonia oxidizers having the capacity to use this substrate.

Here we use a combination of stable isotope tracing, kinetics and transcriptomics studies to resolve the distinct regulatory strategies for selective uptake and metabolism of ammonia and urea by AOA, beta- and gamma-proteobacterial AOB (β-AOB and γ-AOB) and comammox. By revealing that ammonia oxidation and assimilation are both transport dependent, these analyses also provide insights into how reduced N is partitioned between energy generation and biosynthesis, and a mechanistic understanding of previously unrecognized adaptive regulation of cellular affinity for ammonia. Together, these findings advance understanding of niche separation and resource partitioning among lineages of AOM and should foster improved nitrogen cycle models.

Results

AOM lineages exhibit distinct N preferences for catabolism

Comparative analysis of available AOM genomes showed that more than 50%, 60% and 80% of AOA, AOB and comammox species, respectively, contain genes encoding urea permease, urease and accessory proteins (Extended Data Fig. 1). Thus, the potential for urea uptake and utilization is widespread among AOM. Seven phylogenetically and ecologically diverse AOM species, including a marine AOA (*Nitrosopumilus piranensis* D3C)[15], a soil AOA (*Nitrososphaera viennensis* EN76)[16], three β-AOB (*Nitrosospira lacus* APG3, *Nitrosospira multiformis* ATCC 25196 and *Nitrosomonas ureae* Nm10)[17,19,20], a marine γ-AOB (*Nitrosococcus oceani* ATCC 19707)[18] and a comammox (*Nitrospira inopinata* ENR4)[4], were selected for characterization of N substrate preference (Extended Data Fig. 2). As expected, all strains grew by stoichiometric conversion of ammonia or urea to nitrite or nitrate when grown in media containing a single N substrate (Fig. 1). No extracellular urease activity was observed for any of the strains (Supplementary Fig. 1). When grown on mixtures of equal amounts of ammonia- and urea-N, three distinct N utilization patterns emerged (Fig. 1): While the tested AOA and comammox species depleted ammonia before hydrolysing considerable amounts of urea (Fig. 1a–c), β-AOB species used urea before consuming substantial amounts of free ammonia (Fig. 1d–f). In contrast, γ-AOB species simultaneously consumed ammonia and urea (Fig. 1g).

Notably, the marine AOA *N. piranensis* exhibited a marked diauxic lag between the two growth phases (Fig. 1a), reflecting a longer adaptive transition from ammonia to urea consumption. The diauxic lag phase was less pronounced for the soil AOA *N. viennensis*, displaying a rapid transition from ammonia to urea consumption (Fig. 1b). The comammox *N. inopinata* also displayed preferential consumption of ammonia when grown in the mixed N species medium (Fig. 1c). However, *N. inopinata* started to consume urea before the complete exhaustion of ammonia, suggesting a less stringent diauxic transition (Fig. 1c and Supplementary Discussion). During the period of urea consumption, free ammonia concentrations increased in β-AOB *N. lacus* and *N. multiformis* (Fig. 1d,e) and decreased slightly in *N. ureae* cultures (Fig. 1f). Only after near complete consumption of urea did ammonia concentrations decrease substantially (Fig. 1d–f). The same results were observed irrespective of whether cells were pre-grown on either ammonia or urea. Unlike all other tested strains, the γ-AOB *N. oceani* co-utilized ammonia and urea without apparent preference, but only grew on urea at a rate comparable to growth on ammonia in the presence of excess ammonia in the medium (Supplementary Fig. 2). Without ammonia supplementation, *N. oceani* required almost a year to consume 500 μM urea (Fig. 1g and Supplementary Fig. 3), corresponding to an extended average generation time of 23 d.

Consistent with the preferential use of ammonia, characterized AOA and comammox species showed significantly higher specific growth rates ($P < 0.05$) on ammonia, compared with urea after ammonia exhaustion on a mixture of ammonia and urea (Fig. 1a–c). In contrast, the specific growth rates of the β-AOB strains on urea were comparable or even higher ($P < 0.05$) than on ammonia in the mixed medium (Fig. 1d–f), indicating their high urea uptake and hydrolysis activities. Together, these data indicated three contrasting N source preferences and regulation patterns among β-AOB, AOA and comammox, and γ-AOB. Whereas the tested AOA and comammox species repressed the urea-utilizing functions when ammonia was available, β-AOB activated urea transport and hydrolysis rapidly upon exposure to urea.

Although the *Nitrosospira* β-AOB strains preferentially consumed urea, release of free ammonia was observed when grown on urea or a urea–ammonia mixture (Fig. 1d,e). To evaluate the use of free ammonia in the presence of urea, and to investigate the fate of alternative N sources, we used ^{15}N isotope labelling to track conversion of ammonia or urea-N throughout batch culture growth of *N. lacus*, which exhibited the most pronounced release of free ammonia when grown in the mixed medium (Fig. 1d). *N. lacus* was grown on a mixture of ammonia and urea, with one or the other N substrate labelled with ^{15}N. For the $^{15}NH_3$ and ^{15}N-urea tracers, $^{15}NO_2^-$ production was measured (Fig. 2), and for the ^{15}N-urea tracer, $^{15}NH_3$ released to the medium was also measured (Extended Data Fig. 3 and Supplementary Discussion). The temporal distribution of extracellular N isotopes exhibited three distinct phases (Fig. 2). The small amount of $^{15}NO_2^-$ produced during lag phase (0–50 h) originated mostly from $^{15}NH_3$ (Fig. 2a), reflecting metabolism of the ammonia-grown inoculum culture. However, that small amount of $^{15}NO_2^-$ was rapidly diluted by unlabelled nitrite originating from urea throughout exponential growth (~100–150 h), reflecting a sharp drop in $^{15}NH_3$ contribution to $^{15}NO_2^-$ production (Fig. 2a). Conversely, ^{15}N-urea labelling showed that NO_2^- almost exclusively originated from urea in this phase (Fig. 2b). In the presence of ^{15}N-urea, $^{15}NH_3$ was continuously released from cells until urea depletion (Extended Data Fig. 3b). During the third phase following depletion of urea at ~150 h, ammonia consumption rapidly resumed and all nitrite then originated from ammonia until the cessation of growth (Fig. 2a). Collectively, these results provide unequivocal evidence that only the ammonia released from urea hydrolysis in the cytoplasm was oxidized and that the oxidation of extracellular ammonia was repressed in the presence of urea.

https://doi.org/10.1038/s41564-023-01593-7

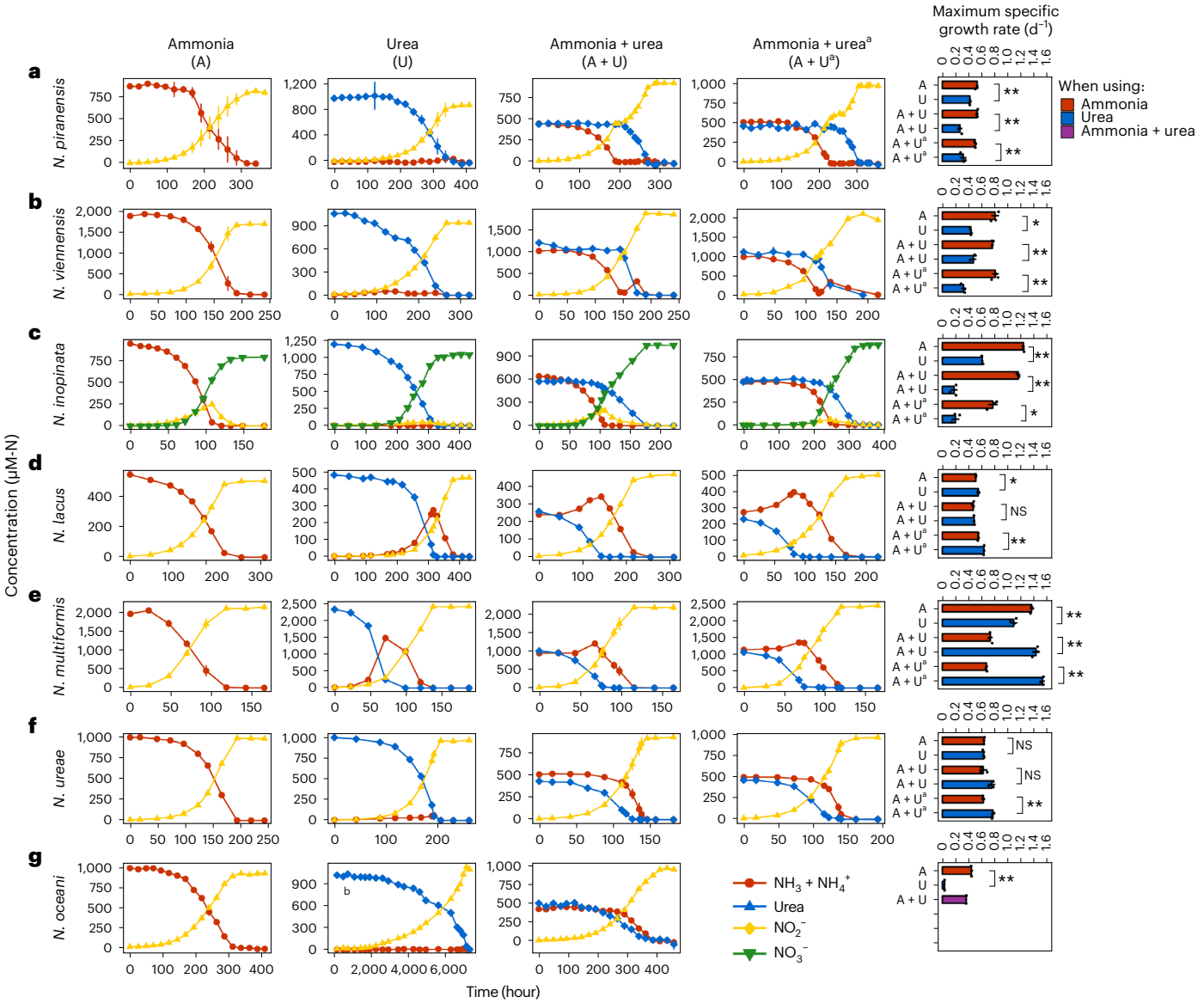

Fig. 1 | Growth curves and maximum specific growth rate (μ_{max}). **a**, *N. piranensis* (marine AOA). **b**, *N. viennensis* (soil AOA). **c**, *N. inopinata* (comammox). **d**, *N. lacus* (*Nitrosospira* β-AOB). **e**, *N. multiformis* (*Nitrosospira* β-AOB). **f**, *N. ureae* (*Nitrosomonas* β-AOB). **g**, *N. oceani* (γ-AOB). [a]Inoculation with 1% urea-grown culture at mid-exponential phase; the other group of incubations on ammonia–urea mixtures were inoculated with 1% ammonia-grown culture. Markers and error bars represent mean ± 1 s.d. of biological triplicates. The s.d. is smaller than the marker if error bar is not visible. [b]Data shown for *N. oceani*'s urea-only incubation from a single incubation without replicates. Urea-only incubations inoculated with urea-grown culture were not conducted for *N. oceani* due to the extremely slow growth rate. Letters indicate incubation with different N substrates: A, ammonia only; U, urea only; A + U, ammonia + urea. For specific growth rate measurements, column heights and error bars represent mean ± 1 s.d. of biological triplicates. Asterisks indicate the range of *P* values calculated from two-tailed *t*-test pairing. $^{**}P < 0.01$; $^{*}0.01 < P < 0.05$; NS, $P > 0.05$ (see Supplementary Table 1 for all *P* values).

Nitrogen of preferred substrate is also used for anabolism

Since ammonia- and urea-N are assimilated by AOM, we also examined their incorporation in representative AOM species at single-cell resolution using stable isotope labelling in combination with nanoscale secondary ion mass spectrometry (NanoSIMS). Following growth on dual-labelled $^{13}C^{15}N$-urea (plus unlabelled NH_3 and bicarbonate) or $^{15}NH_3$ and ^{13}C-bicarbonate (plus unlabelled urea) (Extended Data Figs. 4–7 and Supplementary Fig. 4), cells for NanoSIMS were collected during consumption of the preferred N substrate (T1) and after depletion of all N substrates (T2) (Extended Data Fig. 4a). *N. oceani*, oxidizing both substrates simultaneously, was collected at late-exponential phase (T1) and after both N substrates were exhausted (T2). Urea-derived C was shown to be only a minor carbon source (Extended Data Fig. 7 and Supplementary Discussion).

Although *N. lacus* released substantial ammonia into the medium when using urea, the extracellular ammonia pool was not appreciably assimilated during urea consumption. Results from T1 showed 83.9 ± 6.9% new N incorporation from urea and 16.1 ± 1.4% from ammonia (Extended Data Fig. 4b,c), indicating that urea-N was preferentially assimilated in the first phase of growth. The assimilation of ammonia during the lag phase reflected a period of acclimation of the ammonia-preadapted *N. lacus* to growth on urea–ammonia. At T2, new N incorporation from urea had decreased to 54.2 ± 2.5% and that derived from ammonia had increased to 45.8 ± 1.9% (Extended Data Fig. 4b,c). Thus, even in the presence of free ammonia, urea-derived N was preferentially assimilated by *N. lacus* until urea depletion. A similar set of labelling experiments was performed with the marine AOA *N. piranensis*, soil AOA *N. viennensis* and comammox *N. inopinata*.

https://doi.org/10.1038/s41564-023-01593-7

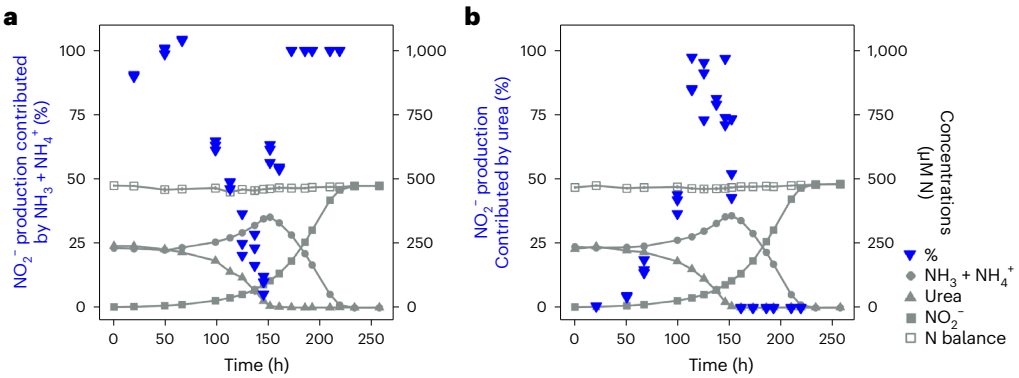

Fig. 2 | ^{15}N stable isotope tracking the ammonia and urea utilization in *N. lacus*. **a**,**b**, The ^{15}N percentage of produced nitrite in the medium was measured for $^{15}NH_3$ tracer incubations (**a**) and ^{15}N-urea tracer incubations (**b**) to calculate the contribution of ammonia and urea to nitrite production. Total concentrations of N species are plotted in light grey on the secondary *y* axis for background reference.

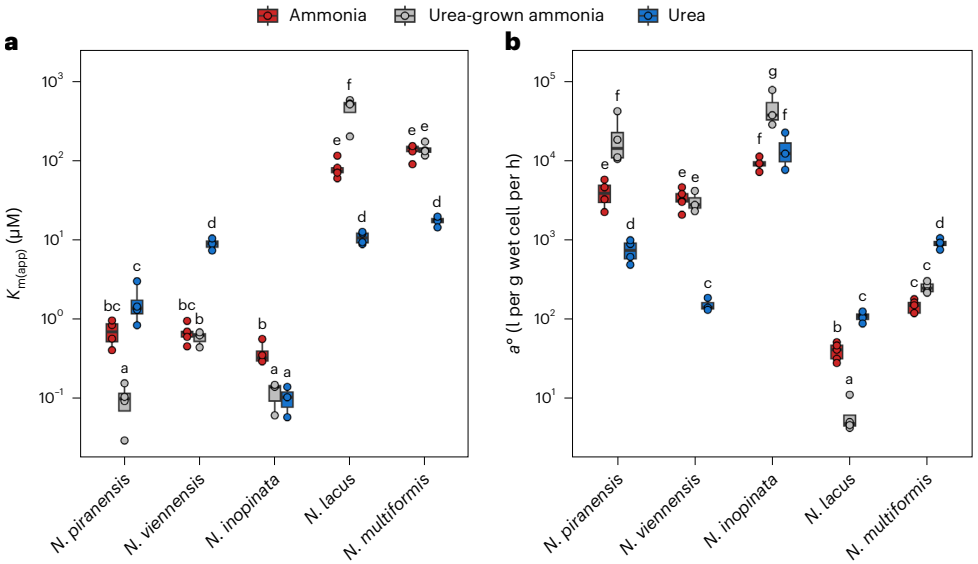

Fig. 3 | Michaelis–Menten kinetic constants of ammonia- and urea-dependent oxidation. **a**, Half-saturation constant ($K_{m(app)}$). **b**, Specific substrate affinity ($a°$). $K_{m(app)}$ and $a°$ for ammonia were determined in both ammonia-grown (red) and urea-grown (grey) cultures, and $K_{m(app)}$ and $a°$ for urea were determined in urea-grown species (blue). The upper limit, middle line and lower limit of the boxplots indicate the 25th, 50th (median) and 75th percentiles, respectively. Dots represent each replicate (n = 3–5 biologically independent experiments). Different lowercase letters denote statistically different groups based on Tukey's HSD after ANOVA comparison of means ($P < 0.05$). Data were $\log_{10}$ transformed to fulfil normal distribution, and Bonferroni correction was used to account for multiple comparisons.

In contrast to *N. lacus*, they all preferentially assimilated N from ammonia (Extended Data Fig. 4b,c and Supplementary Discussion). In addition, γ-AOB *N. oceani* co-assimilated ammonia and urea.

Kinetic characterization of ammonia and urea oxidation

To determine whether N preference was associated with different cellular kinetics, we characterized ammonia- and urea-dependent oxidation kinetics using microrespirometry (Supplementary Table 2). Ammonia and urea-dependent oxygen consumption followed Michaelis–Menten kinetics in all AOM investigated here (Extended Data Fig. 8). Whereas the marine AOA *N. piranensis* showed similar apparent half-saturation constants ($K_{m(app)}$) for ammonia and urea (0.70 ± 0.22 and 1.65 ± 0.82 μM, respectively), the soil AOA *N. viennensis* had comparable $K_{m(app)}$ for ammonia (0.68 ± 0.16 μM), but significantly higher $K_{m(app)}$ for urea (8.97 ± 1.27 μM) (Fig. 3a). Correspondingly, the specific affinities ($a°$) for ammonia and urea in *N. piranensis* and ammonia in *N. viennensis* were similar, whereas *N. viennensis* $a°$ for urea was ~10-fold lower (Fig. 3b). The comammox *N. inopinata* showed comparably high affinity for ammonia as the AOA species. However, unlike the AOA species, *N. inopinata* also showed a very high $a°$ for urea, which exceeds that of *N. piranensis* and *N. viennensis* by >20- and even 90-fold, respectively (Fig. 3b and Supplementary Table 2). *N. inopinata* contains an ABC-type urea transporter (Extended Data Fig. 2) that may support its high affinity for urea via ATP-dependent urea uptake. Notably, the β-AOB *N. lacus* and *N. multiformis* had 2.7–6.2-fold higher $a°$ for urea than for ammonia (Fig. 3b and Supplementary Table 2), comparable to or even higher ($P < 0.05$) than that of *N. viennensis* (Fig. 3b), suggesting that some AOB common in soils and freshwater sediments might effectively compete with AOA for urea.

We further tested ammonia affinities of urea-grown strains. To our surprise, only *N. viennensis* showed similar $K_{m(app)}$ and $a°$ independent of previous growth on ammonia or urea, whereas affinity for ammonia was significantly higher ($P < 0.05$) in urea-grown cells of *N. piranensis* and *N. inopinata* than in ammonia-grown cells (Fig. 3). The capacity of marine AOA and comammox to alter their uptake kinetics for ammonia when growing on urea suggests an adaptation for more efficient uptake

https://doi.org/10.1038/s41564-023-01593-7

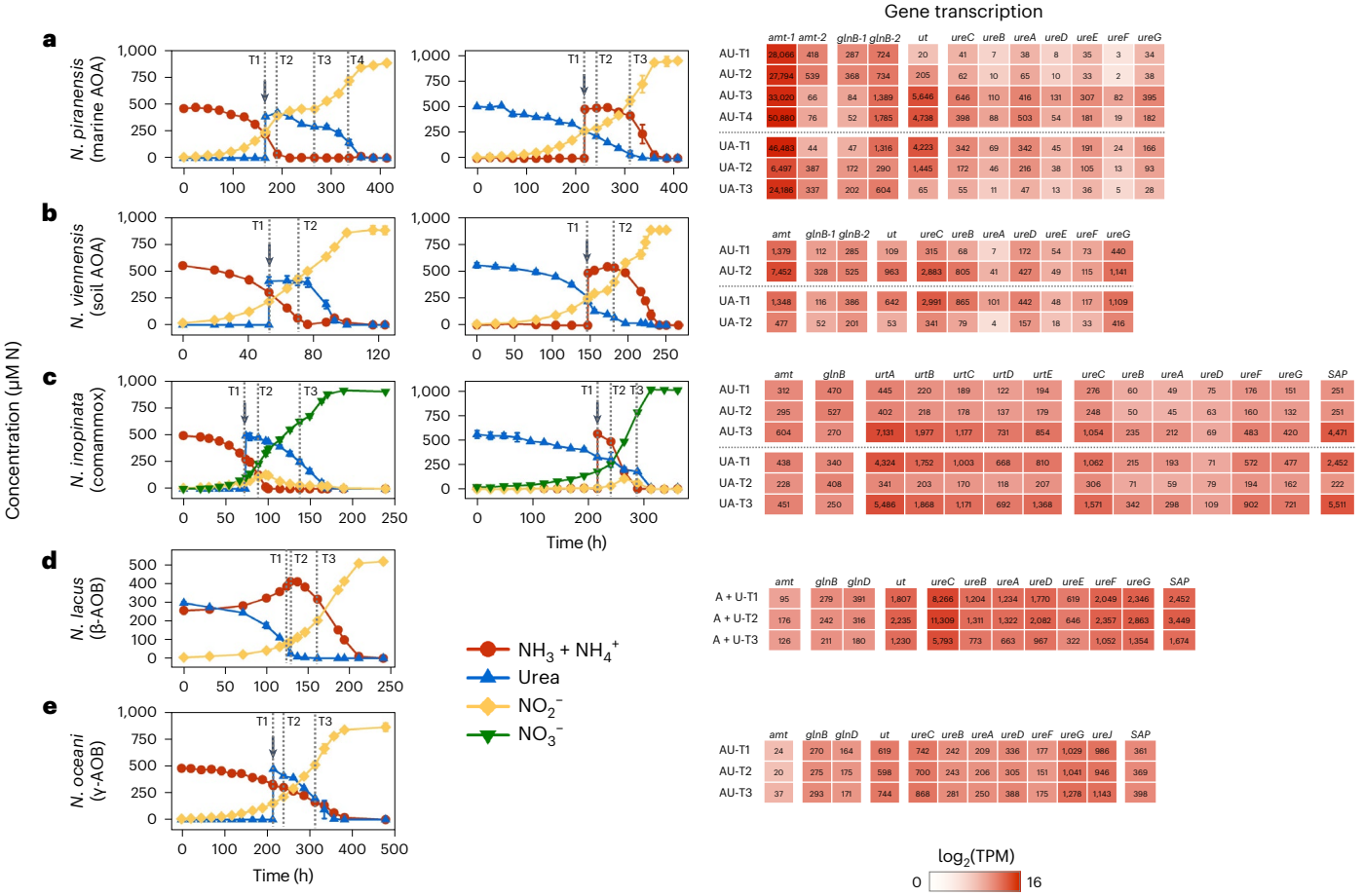

Fig. 4 | Transcriptional response of AOM species to substrate switch from a single N source to a mixture of ammonia and urea. a–e, The transcriptional changes in ammonia- and urea-utilizing genes were investigated 24 h after addition of an alternative N substrate to exponential-phase ammonia-grown (left) or urea-grown (middle) *N. piranensis* (**a**), *N. viennensis* (**b**), *N. inopinata* (**c**), *N. lacus* (**d**) and *N. oceani* (**e**). The growth data showing the times at which the alternative N substrate was added (arrows) and when cells were collected for transcriptomics analysis (dashed lines, T1–T4) are shown on the left and middle. T1 and T2 represent the sampling timepoints before the alternative N substrate addition and at ~24 h after addition, respectively. AU, ammonia-spiked urea; UA, urea-spiked ammonia; A + U, ammonia + urea. Markers and error bars on growth curves represent the mean ± 1 s.d. of biological triplicates. The transcription data for key ammonia- and urea-utilizing genes are profiled on the right. The average TPM values for each gene are shown in coloured boxes and the colour scale bar represents the $\log_2$(TPM). Gene full name and abbreviation pairs, and source data are provided in Supplementary Table 3 and Source Data Table 1, respectively.

of their primary N source. Taken together, the kinetic characteristics of AOM species track their N substrate preferences. *N. inopinata* is a notable exception. Its unusually high urea affinity through ATP-dependent transport might provide competitive advantage in environments where both N sources are available.

Transcription linked to growth on single and mixed N sources

Growth kinetics and gene transcription suggested a regulatory response to the availability of different N sources, as observed for marine AOA *N. piranensis* and soil AOA *N. viennensis* (Fig. 4a,b). Cells were characterized at mid-exponential phase on a single N source (T1) and at 24 h after introduction of the alternative N substrate (T2) (Fig. 4a,b). Additional samples were taken during the extended lag in *N. piranensis* growth during its transition from ammonia to urea (AU-T3) and after its consumption of the newly supplemented N species (AU-T4 and UA-T3) (Fig. 4a).

Among characterized AOA species, ammonia was used as a source of both energy and electrons through its oxidation by ammonia monooxygenase (AMO), and for biosynthesis through the activities of glutamate dehydrogenase (GDH) and glutamine synthetase (GS)[15,25]. Transcription of *amoA* (AMO alpha subunit), *gdh* and *gs* was relatively unchanged during exponential growth of *N. piranensis* and *N. viennensis* on either N substrate (AU-T1 vs UA-T1; Supplementary Table 3). In contrast, the transcription of *amt1* (putative high-affinity ammonium transporter), *ut* (urea transporter), *ure* (urease) and *glnB* (P_{II} protein) were highly responsive to the addition of the alternative N sources (Fig. 4a,b).

Initial low transcription of *ure* and DUR3-type *ut* (NPIRD3C_1395) in ammonia-grown *N. piranensis* increased to very high levels after switching to urea consumption (Fig. 4a). In turn, *ut* transcription was significantly depressed upon addition of ammonia to cultures growing on urea (UA-T2 vs T1, $P = 1.01 \times 10^{-13}$), dropping to its lowest levels when urea was close to depletion (UA-T3). The *amt1* of *N. piranensis* was transcribed at high levels across all growth phases and conditions (Fig. 4a). It was most highly transcribed when growing on urea (46,483 transcripts per million (TPM), UA-T1) and after transitioning to exponential growth on urea (50,880 TPM, AU-T4). Transcript abundance dropped by >7-fold within 24 h after addition of ammonia to urea-grown cultures (6,498 TPM, UA-T2). The increased transcription of *amt1* in urea-grown *N. piranensis* (46,483 TPM, UA-T1) was consistent with our kinetics analyses showing a higher specific affinity for ammonia by urea-grown than by ammonia-grown cells (28,066 TPM, AU-T1) (Fig. 3).

Unlike *N. piranensis*, no differential transcription ($P = 0.84$) of *amt1* (NVIE_002420) was observed between the exponentially growing *N. viennensis* on ammonia (1,379 TPM, AU-T1) and urea (1,348 TPM, UA-T1), consistent with the comparable affinity for ammonia

using either ammonia- or urea-grown cells (Fig. 3). The transcripts of a *ut* (NVIE_014780) and *ureC* (urease alpha subunit, NVIE_014740) located within the same operon were ~10-fold higher or lower within 24 h following addition of urea or ammonia, respectively (AU- and UA-T2 vs T1).

Distinct from the AOA species, the comammox *N. inopinata* exhibited much less stringent control of urea consumption. Urea was hydrolysed immediately upon its addition to ammonia-growing cells (Fig. 4c). As observed for the AOA species, *N. inopinata* significantly increased ($P < 0.01$) the transcription of its single *amt* when transitioning to exponential growth on urea upon ammonia depletion relative to growing on ammonia (AU-T3 vs T1), while its transcript abundance was significantly lower ($P = 6.5 \times 10^{-27}$) 24 h after ammonia addition to urea-grown cells (UA-T2 vs T1). Its significantly higher transcription ($P = 2.8 \times 10^{-3}$) on urea (438 TPM, UA-T1) vs on ammonia (312 TPM, AU-T1) is consistent with the higher ammonia affinity of cells pre-cultured on urea (Fig. 3). Although the *urt* (urea transporter) and *ure* (NITINOP_3355–NITINOP_3362) were transcribed at significantly higher levels ($P = 7.0 \times 10^{-25}$) during exponential growth on urea (UA-T3 vs T1), the cells maintained relatively high transcription levels of these genes when grown on ammonia (Fig. 4c), which is distinct from their extremely low transcription in the marine AOA *N. piranensis* before ammonia depletion (Fig. 4a). Comparable transcription of the *ure/ut* operon and an adjacent gene encoding a putative outer-membrane short-chain amide/urea porin (SAP, NITINOP_3364) in *N. inopinata* (Extended Data Fig. 2) suggests that urea transport is regulated in both outer and inner membranes (Fig. 4c).

Since the substantial free ammonia released during consumption of urea by *N. lacus* would confound the effect of the added ammonia to urea-grown cultures, we instead examined transcript abundance at three timepoints of growth on an ammonia–urea mixture: exponential growth on urea (A + U-T1), near urea depletion (A + U-T2) and after shifting to exponential growth on ammonia (A + U-T3) (Fig. 4d). All genes involved in urea uptake and hydrolysis, including a putative *sap* (EBAPG3_007760), encoded in a single operon (EBAPG3_007760–EBAPG3_007800), were constitutively transcribed at relatively high levels at all timepoints, even when cells were using ammonia (Fig. 4d). This indicates that even while growing on ammonia, β-AOB *N. lacus* allocates substantial resources to facilitate use of its preferred N source urea.

Unlike the highly variable transcription of *amt* observed in the AOA and comammox, a single *N. lacus* Rhesus-type *amt* was always transcribed at low levels in *N. lacus* (Fig. 4d), as has also been observed in *Nitrosomonas* β-AOB and *Nitrosococcus* γ-AOB species[26,27]. Of two genes encoding GlnB-type P_{II} proteins, one (EBAPG3_001140) was transcribed during all growth phases, whereas a paralogue (EBAPG3_010980) showed very limited transcriptional activity. In well-characterized heterotrophs, the transport of ammonia by the AMT can be blocked by its binding to GlnB, controlled by uridylylation/deuridylylation post-translational modification of GlnB by GlnD in response to variations in intracellular energy and N status[28–30]. A *glnD* homologue in *N. lacus* (EBAPG3_003255) suggests that this organism encodes a similar regulatory system. *GlnD* was transcribed at significantly higher levels ($P = 6.6 \times 10^{-15}$) when ammonia utilization was severely repressed (A + U-T1 and T2), suggesting that deuridylylated GlnB binds to AMT and blocks ammonia transport in the presence of urea as shown by isotope tracking (Fig. 2).

Given the extremely slow growth of the marine γ-AOB *N. oceani* on a urea-only medium (Fig. 1g), our transcript analysis only followed the response of cells growing on ammonia with subsequent urea addition. Urea hydrolysis started immediately upon addition and had no substantial effect on the growth rates or the transcription of genes directly involved in N species consumption (Fig. 4e), probably reflecting constitutive systems for ammonia and urea uptake without preference or adaptive lag.

Discussion

The AOM in our study set displayed a wide spectrum of adaptive strategies to coordinate growth on a mixture of urea and ammonia. Among characterized AOM species, AOA and comammox preferred ammonia, β-AOB preferred urea, and γ-AOB co-utilized ammonia and urea (Figs. 1 and 2, Extended Data Fig. 9 and Supplementary Discussion). The preferential use of ammonia is probably a common lifestyle shared among *Nitrosopumilus* and *Nitrososphaera* species, as the characterized genomes of these two AOA clades all encode the putative high-affinity AMT and GlnB-type P_{II} proteins suggested to be associated with efficient ammonia uptake and the repression of urea utilization in AOA, respectively (Extended Data Fig. 1a and Supplementary Discussion). Likewise, the genes involved in the repression of ammonia uptake in β-AOB (*glnB* and *glnD*) are universally present in *Nitrosospira* genomes (Extended Data Fig. 1b), suggesting that a preference for urea may be common among ureolytic *Nitrosospira* species. In contrast, the *glnB* and *glnD* genes are largely absent in most *Nitrosomonas* genomes, which may in part explain the observed weaker repression of ammonia utilization by *Nitrosomonas ureae* compared with *Nitrosospira* species (Fig. 1).

Although distinct lineages of AOM often co-occur in the same environment and variable specific affinity for ammonia is suggested to be the main determinant for competition and niche differentiation[1,6–8,31–34], our study indicates that differences in N substrate prioritization among lineages may mitigate direct competition. For example, β-AOB with a high affinity for urea could prioritize their growth on urea (Fig. 3), while *Nitrosopumilus*/*Nitrososphaera* AOA would thrive in the ammonia-depleted environment due to their much higher affinity for ammonia (Fig. 3, Extended Data Fig. 10 and Supplementary Discussion). We can also now postulate that competitive advantage among *Nitrosopumilus* and related AOA is derived not solely from use of both N substrates, but also from the adaptive capacity of marine AOA to increase their affinity for ammonia upon ammonia exhaustion (Fig. 3), resulting in more efficient scavenging of ammonia released from organic matter decomposition by other microorganisms[35,36].

One of the most important findings of our study is that ammonia oxidation and ammonia assimilation are both transport dependent. Our stable isotope tracking analysis clearly demonstrated that β-AOB did not oxidize extracellular ammonia when growing on a mixture of ammonia and urea. Rather, only ammonia originating in the cytoplasm from urea hydrolysis was oxidized. Ammonia transport is blocked when N needs are satisfied by cytoplasmic hydrolysis of urea, most probably by binding of a GlnB-type P_{II} regulatory protein to the AMT. Thus, these data also implicate an undescribed mechanism for direct or facilitated delivery of cytoplasmic ammonia to the AMO active site.

Since extracellular ammonia must be transported into the cytoplasm by the AMT before being oxidized by the AMO, the AMT must be the rate-limiting functional unit that determines affinity for both the assimilation and oxidation of ammonia among AOM. Although recently determined K_m values of ammonia transporters (for example, ~800 μM for *E. coli* AMT, 3.9 mM at pH 7 for *Archaeoglobus fulgidus* Amt1 (refs. 37–39)) are higher than the cellular $K_{m(app)}$ determined in our study, kinetic data for ammonia assimilation by environmental populations of phytoplankton or heterotrophic bacteria indicate the existence of ammonia transporter variants with higher affinities ($K_{m(app)}$ 0.1–10 μM)[40,41]. Combined modelling and substrate uptake studies of oligotrophic marine bacteria have demonstrated a relationship between the number of cell surface transporters and $a°$ (refs. 42,43). A recent extensive investigation of apparent affinity of different AOM lineages showed that the affinities for ammonia correlate with their cell surface area to volume ratios[8], suggesting that a higher cellular affinity for ammonia is achieved by the higher number of AMTs that can be accommodated on a larger surface area. In our study, a 5.1-fold increase in the $a°$ of *N. piranensis* for ammonia was correlated with increased transcription of its high-affinity AMT (Figs. 3b and 4a). In contrast, the transcription of *amo* remained relatively unchanged

during its exponential growth on either N substrate (AU-T1 vs UA-T1; Supplementary Table 3). Since it is unlikely that a single species can substantially change its cell surface area to volume ratio, the increased cellular ammonia affinity observed for urea-grown *N. piranensis* and *N. inopinata* is most probably caused by the increase in the density of high-affinity AMT per cell surface area.

We recognize that AOM pure cultures representing a broader range of ecotypes are needed to further explore the diversity of N substrate preference and supporting regulatory systems among globally abundant ammonia oxidizers. For example, unlike other AOA lineages, *Nitrosocosmicus* species lack the putative high-affinity AMT (Extended Data Fig. 1a) and exhibit highly active urea hydrolysis activity when grown in urea-only media[44], which suggests that their regulation of N substrate utilization is distinct from that of *Nitrosopumilus* and *Nitrososphaera* species. In addition, while both clade A and clade B comammox species possess ATP-dependent urea transporters, they differ in their encoded ammonia transporter types and the presence of GlnD proteins[45] (Extended Data Fig. 1c). As more diverse comammox strains become available, it will be interesting to see whether different transporter inventories impact the regulatory mechanisms controlling N catabolite repression.

In summary, our study revealed an unexpected diversity in substrate preference and supporting regulatory systems among AOM and has markedly changed our understanding of their ecophysiology and niche differentiation. Our surprising finding that ammonia oxidation is transport dependent suggests the need for modifying current models of ammonia oxidation. Our finding that cellular ammonia affinity is not an intrinsic property of AOA and comammox species, but a property that can be adaptively regulated in response to the environmental ammonia availability, has implications on how N resource competition is modelled among AOM groups. Adding these novelties to models will ultimately offer a more holistic and accurate representation of N resource partitioning among AOM in natural and engineered systems.

Methods

Laboratory strains

Nitrososphaera viennensis strain EN76 was obtained from the German Type and Culture Collection (DSMZ). *Nitrosopumilus piranensis* strain D3C was kindly provided by Dr Alyson Santoro and Dr Barbara Bayer (University of California, Santa Barbara), and *Nitrosomonas ureae* strain Nm10 was kindly provided by Dr Andreas Pommerening-Röser (University of Hamburg). *Nitrosospira multiformis* strain ATCC 25196 was kindly provided to the University of Oklahoma by Dr Jeanette Norton (Utah State University). *Nitrosospira lacus* strain APG3 was isolated from Green Lake in Seattle, Washington. *Nitrosococcus oceani* strain ATCC 19707 was obtained from the American Type Culture Collection (ATCC). *Nitrospira inopinata* strain ENR4 was kindly provided to the University of Washington by Dr Holger Daims (University of Vienna). For measurements (such as the affinity measurements) at all other locations, *N. inopinata* was obtained from DSMZ.

Cell maintenance

Pure cultures of marine AOA *N. piranensis* and marine γ-AOB *N. oceani* were maintained in HEPES-buffered synthetic Crenarchaeota medium, and soil AOA *N. viennensis*, comammox *N. inopinata*, β-AOB *Nitrosospira lacus*, *Nitrosospira multiformis* and *Nitrosomonas ureae* were maintained in HEPES-buffered freshwater medium[46,47]. All media pH were 7.6–7.8. All stock cultures were grown in 250 ml bottles containing 100 ml medium supplemented with ammonia or urea in the dark to avoid light inhibition. *N. viennensis* and *N. piranensis* were additionally supplemented with 100 µM sodium pyruvate as a scavenger for hydrogen peroxide (H_2O_2) or other reactive oxygen species. All cultures were grown without agitation except *N. oceani*, which was grown with a shaking speed of 70 r.p.m. *N. piranensis*, *N. viennensis*, *N. inopinata*, *N. lacus*, *N. multiformis*, *N. ureae* and *N. oceani* were incubated at 30 °C, 42 °C, 37 °C, 20 °C, 28 °C, 25 °C and 25 °C, respectively. The medium was pre-warmed to culturing temperature before inoculation to avoid lower growth rates induced by temperature shock. Growth was monitored by ammonia or urea consumption as well as nitrite or nitrate accumulation. When mid- to late-exponential phase was reached, 0.5–1% inoculum was transferred to fresh media.

Culture purity was confirmed monthly by the absence of growth on R2A agar and (marine) LB broth. Sanger sequencing of 16S ribosomal (r)RNA genes was conducted every 6 months to confirm purity of the strains.

Growth experiments on single and mixed N substrates

Growth experiments. Incubation experiments were set up with three different conditions: ammonia only, urea only and ammonia plus urea. Inoculation was done with 0.5–1% transfer from the maintenance culture at mid-exponential phase. The inocula used for the ammonia-only and urea-only experiments were transferred from the maintenance culture growing in media containing ammonia or urea as the only N substrate, respectively. The ammonia plus urea experiment was conducted with both ammonia- and urea-grown maintenance cultures. Media composition, culture volume and growth conditions were the same as for the maintenance cultures. A negative control bottle was prepared for the urea-only and ammonia plus urea treatments without addition of cells to confirm negligible non-biological degradation of urea during experimental periods. Samples were taken roughly at every doubling time for nutrient measurements (urea, NH_3, NO_2^- and NO_3^-). Specific growth rates (μ) were determined from the log linear region of NO_2^- or NO_2^- + NO_3^- production for AOA/AOB or comammox, respectively (Supplementary Fig. 5). AOM culture purity checks were performed at the end of each growth experiment. No growth was detected on R2A agar or (marine) LB broth, indicating the absence of contaminants. In addition, transcriptomics data analysis did not identify any contaminant transcripts.

Cell count. A mounting medium was prepared consisting of 3 µl 1 mol l^{-1} ascorbic acid and 4 µl of SYBR Green I stock solution (10,000-fold concentrated in DMSO, equivalent to 10 mmol l^{-1}) in 200 µl of Moviol solution (Moviol 4-88; Fluka)[48]. Cells were captured on a 0.02 µm Anopore membrane filter (Whatman) and stained with 20 µl of the mounting medium. Using a Zeiss Axioskop 2 MOT epifluorescence microscope (Carl Zeiss) (for freshwater and soil AOM experiments) and Nikon Eclipse Ni microscope (for marine AOM experiments), cell numbers were determined for 20 random fields (20–100 cells per field) per sample.

No discernible large cell aggregates were observed for *N. piranensis*, *N. viennensis*, *N. inopinata*, *N. lacus* and *N. ureae* under the tested growth conditions in this study. Cell aggregates were occasionally observed for *N. oceani* growing in urea-only media, which could be attributed to extremely slow growth on urea (Fig. 1g) and potential stress response. To ensure accurate cell counts, the urea-grown *N. oceani* cultures were meticulously pipetted up and down to disperse any possible cell aggregates before collecting cells for cell counts. Some cell aggregates were observed in growth experiments of *N. multiformis* without agitation, which may be attributed to oxygen limitation caused by rapid O_2 consumption during high rates of ammonia oxidation. For cell counts, each culture sample was passed through a syringe and needle (0.4 mm diameter) at least three times to disperse aggregated cells following a previously described method[44]. In contrast, no aggregates were observed during kinetics measurements (see details below) using microrespirometry chambers with continuous stirring to maintain O_2 homogeneity.

Extracellular urease activity check. Incubation experiments were conducted to check whether urease activities occurred extracellularly. Cultures were grown to early stationary phase in urea-only media using the same volume and growth conditions as the maintenance cultures. The same cultures were then filtered through 0.2 µm PES filter

membrane (Pall Supor), preventing AOM cells from passing through and leaving only remaining active urease enzymes, if any, in the filtrate. The filtrates were supplemented with additional urea, and concentrations of ammonia and urea were monitored for 1–2 weeks to check for extracellular urease activity.

Chemical analysis. Nitrite was measured spectrophotometrically using the sulfanilamide and *N*-(1-naphthyl)-ethylenediamine dihydrochloride method (EPA Method 354.1). Ammonia concentrations were either determined colorimetrically from the monochloramine generated by the reaction with alkaline hydrolysis of sodium dichloroisocyanurate (ISO 15923-1) or using the *o*-phthaldialdehyde fluorescence method[49]. For determination of nitrate, NO_3^- was first reduced to NO_2^- by hydrazine or vanadium chloride[50], then the procedure for NO_2^- measurement was followed to determine the total oxidized N (TON). NO_3^- was determined from TON minus NO_2^-. Urea was measured according to previously described protocols[51]. First, an aliquot was split from the original sample and treated with urease (Millipore Sigma, U1500) to convert urea into ammonia. Ammonia was measured for the urease-treated aliquot and the original sample. Urea-N was then determined by subtracting the ammonia concentration in the original sample (untreated) from that in the aliquot (urease-treated).

^{15}N label tracking for ammonia oxidation

Incubation with labelled substrates. Cells were incubated as described in 'Cell maintenance' with additional details provided in this section. All incubations were done in ammonia plus urea medium (1:1 N molar ratio) but with different substrates labelled. One set of experiments was conducted with ~5% ^{15}N-ammonium chloride (Sigma-Aldrich, 299251) (and 95% unlabelled ammonia) for the *N. piranensis*, *N. viennensis*, *N. lacus* and *N. oceani* incubations. The other set of experiments was conducted with ~5% ^{15}N-urea (Sigma-Aldrich, 316830) (and 95% unlabelled urea) for these four AOM species. Given that no observable effect on the ammonia oxidation activity was detected when varying ^{15}N labelling percentages from 1 to 10% (Supplementary Fig. 6), the labelling incubation experiments for *N. inopinata* were conducted using a lower ^{15}N labelling percentage (~2.5% $^{15}NH_4Cl$ or ~2.5% ^{15}N-urea) compared with the other tested AOM species; this allowed us to obtain a more appropriate range of δ^{15}N signals for accurate measurement using the GC–IRMS system (see detailed methods below). Three or four parallel incubations were set up for biological replicates and nutrient measurements. Four millilitres of cultures were collected at each timepoint, with 2 ml being used for nutrient measurements and the other 2 ml being filter-sterilized using a 0.2 µm syringe-driven filter into a microcentrifuge tube and immediately frozen at −80 °C for isotope analysis.

δ^{15}N of NH_4^+, NO_2^- and NO_3^-. δ^{15}N of NO_2^- for *N. lacus* and *N. oceani* incubations was measured by chemical conversion (sodium azide, Sigma-Aldrich) of NO_2^- to N_2O[52]. δ^{15}N of NO_X^- (NO_2^- plus NO_3^-) for *N. inopinata* incubation was determined using the bacterial denitrifier method[53]. δ^{15}N of the N_2O converted either through chemical conversion or denitrifier reduction was quantified using a GC–IRMS system (a cryogenic extraction and purification system interfaced to a Delta V isotopic ratio mass spectrometer)[54]. δ^{15}N of NO_2^- was calibrated against five in-house NO_2^- standards (δ^{15}N of the five in-house NO_2^- standards were 5.19‰, 126.07‰, 336.54‰, 671.78‰, 1,343.28‰, respectively). δ^{15}N of NO_3^- values were calibrated against NO_3^- isotope standards USGS 34, IAEA N3 and USGS 32. Standard curves were run at the beginning and end of sample analysis and at 10 sample intervals.

For δ^{15}N of NH_4^+, the samples were measured using hypobromite oxidation coupled to the azide conversion method[55] with slight modification[56]. Before the NH_4^+ was oxidized to NO_2^-, the pre-existing NO_2^- was removed from samples using sulfamic acid (≥99% sulfamic acid, Sigma-Aldrich)[57]. The removal efficiency of NO_2^- was tested by measuring the NO_2^- concentration before and after adding the sulfamic acid to 10 µmol l^{-1} of NO_2^-, and the oxidation efficiency of NH_4^+ to NO_2^- was tested by comparing the NH_4^+ and NO_2^- concentrations before and after hypobromite oxidation, with initial NH_4^+ concentration of 2 µmol l^{-1}. The NO_2^- removal and NH_4^+ oxidation efficiencies in our experiments were >99% and >90%, respectively. All the samples were diluted to the NH_4^+ concentration of 2 µmol l^{-1} for hypobromite oxidation. δ^{15}N of NH_4^+ was calibrated against five in-house NH_4^+ standards (δ^{15}N of the five in-house NH_4^+ standards were 0.31‰, 135.04‰, 326.07‰, 588.08‰, 1,324.84‰, respectively). Standard curves were run at the beginning and end of sample analysis and at 10 sample intervals.

Contribution of NO_X^- from NH_4^+ and urea. The contribution of NH_4^+ (or urea) to NO_2^- production for *N. lacus* and *N. oceani* incubations, and to NO_X^- production for *N. inopinata* incubation was calculated on the basis of the isotopic mass balance model at each timepoint. Briefly, δ^{15}N of the net produced NO_2^- between two consecutive timepoints during the time course of incubation was calculated using a two-end member mixing model (equation 1):

$$\delta^{15}N_{NO_2} = \frac{C_{t2} \times \delta^{15}N_{NO_2t2} - C_{t1} \times \delta^{15}N_{NO_2t1}}{C_{t2} - C_{t1}} \quad (1)$$

where $\delta^{15}N_{NO_2}$, $\delta^{15}N_{NO_2t2}$ and $\delta^{15}N_{NO_2t1}$ denote the $\delta^{15}N_{NO_2^-}$ value of the net produced NO_2^- during the $^{15}NH_4^+$ or ^{15}N-urea labelling incubation, and the $\delta^{15}N_{NO_2^-}$ at two consecutive timepoints, respectively. C_{t2} and C_{t1} denote the measured NO_2^- concentration at the two timepoints, respectively.

The fraction contributions of the net produced NO_2^- by NH_4^+ and urea between two consecutive timepoints were derived using equation (2):

$$AT^{15}N_{NO_2^-} = AT^{15}N_{NH_4^+} \times a\% + AT^{15}N_{urea} \times (100\% - a\%) \quad (2)$$

where $AT^{15}N_{NO_2^-}$ is the fraction of ^{15}N atom (%) of the net produced NO_2^- between two timepoints, which is calculated using the $\delta^{15}N_{NO_2}$ in equation (1). $AT^{15}N_{NO_2^-}$ and $AT^{15}N_{urea}$ are the fractions of ^{15}N atom (%) in the NH_4^+ and urea pool of the corresponding timepoint (refer to t1 in equation 1). a% denotes the fractional contribution of NH_4^+ to the net produced NO_2^- at the corresponding timepoint.

Tracing the sources of N and C for assimilation by NanoSIMS analysis

Incubation with labelled substrates. Cells were incubated as described in 'Cell maintenance' except as detailed in this section. All incubations were done in ammonia plus urea medium (1:1 N molar ratio) but with different substrates labelled. One set of experiments used ^{15}N-ammonium chloride (Sigma-Aldrich, 299251) and ^{13}C-sodium bicarbonate (Cambridge Isotope Laboratories, CLM-441-5), and the other set used $^{15}N^{13}$C-dual-labelled urea (Sigma-Aldrich, 490954). We used 100% labelled compounds for *N. viennensis*, *N. inopinata*, *N. lacus* and *N. oceani* incubations. Since the fully labelled compounds inhibited the growth of *N. piranensis*, 30% labelled compounds were used.

For *N. viennensis*, *N. inopinata* and *N. lacus*, cells were collected for the first timepoint when the preferred N substrate was consumed and for the second timepoint when both N substrates were depleted. For *N. piranensis*, cells were collected for the first timepoint during exponential growth using ammonia and the second timepoint when both ammonia and urea were exhausted. For *N. oceani*, which co-utilized ammonia and urea, cells were collected at late-exponential phase and stationary phase for the first and second timepoints, respectively. Growth was monitored by measuring ammonia and urea consumption and nitrite/nitrate accumulation. Parallel incubations (8–12) were set up for biological replicates, and cells were collected and fixed (>9×10^6 cells) from 3–4 replicate cultures at each timepoint for NanoSIMS

analysis. An unlabelled control was prepared with all unlabelled media components, and a killed control was prepared with all labelled media components and a 2% (v/v) paraformaldehyde-killed inoculum. Before adding the killed inoculum, cells were pelleted at 10,000 × *g* at 20 °C for 1 h and resuspended in a standard 1× phosphate buffered saline solution. This step was repeated two more times to remove residual paraformaldehyde.

Cells were collected and fixed in 2% (v/v) paraformaldehyde at room temperature in the dark for 30–40 min, diluted with sterilized Milli-Q water for a target of 10 million cells, then filtered onto a 25-mm-diameter 0.2-µm-pore-size polycarbonate membrane (Millipore Sigma, GTTP02500) using vacuum filtration. Cells were then washed three times with sterile filtered Milli-Q water to remove residual labelled media. The filter was put in a single well of a 12-well plate (sample side facing up) (Thermo Fisher) and stored at 4 °C in the dark for subsequent NanoSIMS analysis.

Dissolved inorganic carbon measurement. Three media samples for both labelled treatments (30 ml), an unlabelled media control sample and an atmospheric gas control sample were collected in 50 ml sealed serum bottles for dissolved inorganic carbon (DIC) analysis. In addition, 3 unfixed culture samples were taken at each timepoint and stored at 4 °C for ^{13}C DIC measurement. These liquid samples were acidified with HCl, driving all DIC into CO_2. Headspace gas was collected for isotopic gas analysis using a G2201-I Cavity Ring Down spectrometer (Picarro). Vials were initially autoclaved and filled with one atmosphere of nitrogen gas before addition of 5 ml of gaseous sample headspace. Each vial then had 5 ml of gaseous headspace removed using a gas-tight syringe injected into the small sample introduction module 2. The factory protocol was then run with a zero-air dilution and analysed for $^{13}CO_2/^{12}CO_2$. Ambient air was used after every third injection as a reference point for calibration and to ensure lack of instrument drift.

NanoSIMS. Filters were cut into wedges of 1/8 size using sterile scissors, adhered to aluminum discs using conductive tabs (16084-6, Ted Pella) and sputter coated with ~5 nm of gold. Isotope imaging was performed with a CAMECA NanoSIMS 50 at Lawrence Livermore National Laboratory. The primary $^{133}Cs^+$ ion beam was set to 1.5 pA, corresponding to a ~150-nm-diameter beam at 16 keV. Rastering was performed over 20 × 20 µm analysis areas with a dwell time of 1 ms pixel^{-1} for 19–30 scans (cycles) and generated images containing 256 × 256 pixels. Sputtering equilibrium at each analysis area was achieved with an initial beam current of 90 pA to a depth of ~60 nm. After tuning the secondary ion mass spectrometer for mass resolving power of ~7,000 (1.5× corrected), secondary electron images and quantitative secondary ion images were simultaneously collected for $^{12}C_2^-$, $^{13}C^{12}C^-$, $^{12}C^{14}N^-$ and $^{12}C^{15}N^-$ on individual electron multipliers in pulse counting mode; $^{13}C^{12}C^-/^{12}C_2^- = 2 \times {}^{13}C/{}^{12}C$ and $^{12}C^{15}N^-/^{12}C^{14}N^- = {}^{15}N/{}^{14}N$[58]. All NanoSIMS datasets were initially processed using L'Image (http://limagesoftware.net) to perform dead time and image shift correction of ion image data before creating $^{13}C/^{12}C$ and $^{15}N/^{14}N$ ratio images, which reflected the level of ^{13}C and ^{15}N incorporation into biomass. To quantify substrate incorporation, cells were identified on the basis of $^{12}C^{14}N^-$ images, and regions of interest (ROIs) for cells were drawn with the automated algorithm. The automatic particle analysis algorithm has no difficulty in separating cells from one another. The isotopic ratio averages and standard error of the mean for each ROI were calculated from ratios by cycle. Excess fraction of cellular C and N incorporated in cells from the enriched isotopic substrate (C_{net} and N_{net}, respectively) was calculated on the basis of the isotope fraction in a target cell (F_c), the killed controls (F_{kc}) to represent the initial enrichment of the cells, and the isotope fraction of the added substrates (F_s), according to equation (3)[59]:

$$[\text{C or N}]_{net} = \frac{F_c - F_{kc}}{F_s - F_{kc}} \quad (3)$$

The ROI data were exported for further statistical analyses in R, which was used to calculate the mean and standard error of the mean C_{net} and N_{net} for each treatment and timepoint. Subsequently, % new N incorporation from urea or ammonia and % new C incorporation from urea or bicarbonate were calculated; for example, % new N incorporation from urea = N_{net}urea/(N_{net}urea + N_{net}ammonia).

Affinity and kinetics measurements

Cell maintenance. Cells were maintained as described in 'Cell maintenance', except that transfer was done with 5% v/v inoculum and culture volume was 200 ml in 1 l glass bottles. Each strain was maintained with either 1.0 mM NH_4Cl or 0.5 mM urea and was used separately to determine oxidation kinetics. *N. piranensis* and *N. viennensis* cultures were additionally supplemented with 100 µM α-ketoglutaric acid and 500 µM sodium pyruvate, respectively, as H_2O_2 scavengers.

Substrate-dependent oxygen uptake. Substrate oxidation kinetics were measured using a microrespirometry (MR) system setup described previously[60]. Briefly, the setup was equipped with 80 ml three-port glass MR chambers (Unisense), a magnetic stir bar and an OX-MR oxygen microsensor (Unisense). Sensors were polarized and pA signals were amplified and converted to mV using PA2000 picoammeters (Unisense). Data were recorded at 1 Hz using a Lab-Trax-4/16 data acquisition system (World Precision Instruments) and LabScribe v.4.0 (iWorks). Oxygen sensors were continuously polarized before use and calibrated using culture media equilibrated with laboratory air and oxygen-free water in a 4 ml calibration chamber (Unisense) for zero reading according to manufacturer recommendations. All measurements were done in a recirculated water bath at the optimal growth temperature for each strain.

Nitrite concentrations in cell cultures were monitored daily and early-stationary-phase cells (culture pH 7.3–7.5) were transferred directly into the MR chamber upon N substrate (ammonia or urea) depletion to minimize perturbations as previously described[6]. *N. inopinata* cells were transferred when both NH_3 and NO_2^- were depleted. The chamber was filled with culture to overflowing and closed with MR injection lids to ensure that no headspace was left. For *N. viennensis*, 50 mg l^{-1} kanamycin was added to the chamber after culture transfer to avoid bacterial contamination. Background sensor signal drift was measured for 30–60 min before initial substrate injections. Cells were initially activated by addition of 5 µM NH_4Cl or 5 µM urea, depending on which substrate cells were grown with. To obtain O_2 uptake traces for kinetic parameter determination, 20–40 µM NH_4Cl were injected next and O_2 uptake was recorded until at least 30 min after substrate depletion. Subsequently, 10–20 µM urea was injected for urea-dependent kinetics measurements. For *N. lacus* and *N. multiformis*, measurements described above yielded no discernible activities. Therefore, measurements with discrete substrate additions were conducted as follows. Initial O_2 uptake was recorded for at least 30 min with multiple ammonia (5 µM–10 mM) or urea (2.5–500 µM) injections to cover the large substrate concentration range required for determination of kinetic constants in these strains.

Cell counting and estimation of protein content. Cells used for MR measurements were filtered onto 0.2 µm black polycarbonate membranes (Millipore Sigma) for cell counts. Filters were air-dried and mounted with SYBR Green I (Invitrogen) in Moviol mounting solution, incubated at −20 °C for at least 2 h and counted by epifluorescence microscopy[48]. Cell volumes were calculated using previously reported cell diameter and length of each strain[4,15,20,47,17]. Protein contents for each strain were estimated on the basis of protein to cell volume ratios[61].

Calculation of kinetic constants. O_2 uptake traces were used to determine kinetic constants for the tested AOM strains. Substrate to O_2 consumption stoichiometry ratios of 1:1.5 using total ammonia

(NH_3 + NH_4^+) and 1:3 using urea were used to calculate N substrate concentrations at a given O_2 uptake rate. For *N. inopinata*, the expected stoichiometry of total ammonia to O_2 was 1:2 (ref. 7). However, in this study we found that at low ammonia concentrations, *N. inopinata* oxidized NH_3 to only NO_2^- and not NO_3^-, hence only 1.5 mol of O_2 was consumed per mol N of NH_3 or urea substrate under measurement conditions, where NO_2^- concentrations remained far below its $K_{m(app)}$ for NO_2^-. Kinetic constants were obtained by fitting a Michaelis–Menten equation to total ammonia or urea and oxidation rates using equation (4):

$$V = (V_{max} \times [S]) \times (K_{m(app)} + [S])^{-1} \quad (4)$$

where V refers to the rate of oxygen uptake (in μmol mg protein^{-1} h^{-1}), V_{max} is the maximum rate of oxygen uptake (μmol mg protein^{-1} h^{-1}), S is the concentration of substrate (μM) and $K_{m(app)}$ is the concentration of N substrate at which half of the maximum rate is achieved (μM). $K_{m(app)}$ and V_{max} values for total ammonia and urea were calculated in NH_3^- and urea-grown strains, respectively. Specific affinities were calculated from kinetic constants for each strain using equation (5):

$$a^\circ = V_{max} \times K_{m(app)}{}^{-1} \quad (5)$$

where a° is specific affinity (l per g wet cell per h), V_{max} values were normalized to protein concentration (μmol N per mg protein per h) and $K_{m(app)}$ is the apparent half-saturation constant (μmol l^{-1}). The factor of 5.7 g wet weight per g protein was used to estimate wet weight from protein content[42,6]. All measurements were carried out in at least ten replicates to obtain at least three replicates with low-enough noise for subsequent calculation of kinetic constants. Each trace was manually inspected for stirring noise and only the three to four traces with the least noise were subjected to downstream kinetic analyses. Replicates for each strain were generated over a 2–4-week timeframe with no more than 2 out of 10 traces originating from the same culture. Kinetic constants ($K_{m(app)}$ and a°) ranged over several orders of magnitude and Levene's test showed that residuals were not homogeneous. Therefore, $K_{m(app)}$ and a° data were $\log_{10}$ transformed to satisfy parametric test assumptions. Comparisons of means were then conducted by one-way analysis of variance (ANOVA). Kinetic constants for ammonia in ammonia-grown strains and kinetic constants for ammonia and urea in urea-grown strains were compared as a factor, yielding 12 groups. Statistically different groups were determined using Tukey's HSD post-hoc analysis ($\alpha = 0.05$) with Bonferroni correction. Statistical analyses were performed using SPSS 21 (IBM SPSS 2016) and R v.3.6.3.

Transcriptomics analysis

Alternative nitrogen substrate spiking experiment. To capture the regulatory response of AOM to switches between ammonia and urea utilization, incubations were conducted with one initial N substrate and spiked with the second N substrate via two directions: (1) incubation with initially ammonia then spiked with urea (AU) and (2) incubation with initially urea then spiked with ammonia (UA). Because ammonia was secreted out of the cells during urea consumption in *N. lacus* incubations, *N. lacus* was instead grown on a mixture of ammonia and urea (A + U). All media and growth conditions were the same as described in 'Cell maintenance', except that incubations were done in larger volumes to obtain enough cell material for RNA extraction. For each experiment, 12–18 parallel incubations of 400 ml cultures were grown in 2 l bottles, except for *N. lacus* which was grown in 800 ml culture volumes in 2 l bottles to maximize cell material. Preliminary incubation was conducted with 800 ml *N. lacus* cultures to confirm no oxygen limitation. The inocula used for the AU experiments were transferred from ammonia-grown maintenance culture, whereas urea-grown maintenance culture was used as inoculum for the UA experiments.

Cell collection. For each replicate RNA sample, the entire culture from 1 or 2 bottles (each with 400 ml culture) was filtered onto Supor 0.2 μm 47 mm membrane filters (Pall). The filters were immediately flash frozen and stored at −80 °C until RNA extraction. Each timepoint had 4 replicate RNA samples. Due to the differences in physiological response to alternative N substrate addition, the collected timepoints differed for each AOM and are summarized in Supplementary Table 4.

RNA extraction and RNA sequencing. For each timepoint, RNA was extracted from four biological replicates following a manual phenol–chloroform RNA extraction method as previously described[62]. Briefly, the entire membrane filter (with cells collected) was dissolved in an extraction buffer containing 21 mM sodium acetate, 0.6 mM EDTA, 0.6% SDS and 51% (v/v) phenol solution preheated to 80 °C (saturated with 0.1 M citrate buffer, pH 4.3; Fisher Scientific). The samples were disrupted with a bead beater (MP Biomedical) at 4 m s^{-1} for 30 s and spun down. The supernatant was treated with equal volume of phenol/chloroform/isoamyl alcohol (125:24:1) (pH 4.5, Fisher Scientific). The bead beating, spinning down and treatment steps were repeated with chloroform:isoamyl alcohol (24:1) (Sigma-Aldrich). The final supernatant was treated with 0.8 M lithium chloride and equal volume of 100% isopropanol, and precipitated for RNA at −80 °C overnight. The precipitant was pelleted by centrifugation, washed with 75% ethanol and dried at room temperature. The RNA pellet was then dissolved in RNase-free water. The RNA sample was treated twice with Ambion's DNA-free DNA removal kit, and the precipitation steps with lithium chloride and overnight precipitation at −80 °C were performed again. The final RNA was recovered using the MP spin column (MP Biomedical), washed twice with 75% ethanol and eluted with RNase-free water.

The DNA contaminant removal efficiency was verified by qPCR analysis showing no or very low amplification copy number. The concentrations and quality of RNA samples were checked with an Agilent 2100 bioanalyser. The three replicates with the highest RNA integrity numbers were shipped to Azenta Life Science (New Jersey, USA) for rRNA depletion with the QiaSeq FastSelect kit (Qiagen, 335921), library preparation and sequencing on the Illumina HiSeq 2000 platform. About 18 RNA samples were sequenced per HiSeq lane at ~5 GB data per sample.

Gene transcription analysis. Raw reads were trimmed using Trimmomatic (v.0.36)[63] and clean reads were aligned with the reference AOM species genomes using Bowtie2 (v.2.3.4)[64]. The alignments were postprocessed into sorted BAM files with Samtools (v.0.1.19)[65]. Reads were attributed to open reading frames using the htseq count tool of HTseq 2.0 (ref. 66). TPM values were calculated using equation (6):

$$\mathrm{TPM} = \frac{\mathrm{rg} \times \mathrm{rl} \times 10^6}{\mathrm{cl} \times T} \quad (6)$$

where rg is reads mapped to gene g, rl is read length, cl is coding sequence length and T is the sum of rg × rl × cl^{-1} for all genes. Differential abundance analysis was performed with DESeq2 (v.1.2.10)[67].

Comparative genomics analysis

All publicly available and published AOM genomes were downloaded from the NCBI Refseq database as of 7 June 2023. Only high-quality genomes with a completeness ≥90% and contamination ≤5%[68] were chosen, and the selected genomes were further clustered using a multistep distance-based approach with an average nucleotide identity threshold of 95% over at least a 30% alignment fraction by dRep (v.3.4.2)[69]. From each cluster, the best-quality genome was selected as the representative for comparative analysis, considering factors such as genome completeness, minimal contamination and assembly N50 (the average length of contigs representing the midpoint of the assembled sequence dataset) (with culture genomes always given

preference over metagenome-assembled genomes). The encoded protein sequences of 136 AOA, 92 AOB and 61 comammox culture genomes and metagenome-assembled genomes were searched via diamond (v.0.9.24.125)[70] with an *E*-value of $\leq 1 \times 10^{-5}$, identity of ≥50% and coverage of ≥50% against an in-house database of ammonia and urea uptake and utilization genes found in the KEGG database. Completeness and contamination levels of AOM genomes were assessed using CheckM (v.1.0.18)[71]. SignalP 6.0 (ref. 72) was utilized to predict the presence of signal peptides in the urease enzyme of the tested AOM species. The phylogenomic trees of AOA, AOB and comammox species were constructed on the basis of concatenated alignments of marker proteins from the GTDB database[73]. The concatenated alignments were constructed using GTDB-Tk (v.2.0.0)[74] and the trees were built using IQ-TREE (v. 2.1.2 COVID-edition)[75] with 1,000 times ultrafast bootstrapping.

Statistics and reproducibility

Statistics for kinetic analysis were performed using one-way ANOVA, and differential abundance analysis for transcriptomics studies was performed with DESeq2 (v.1.2.10)[67]. No statistical method was used to predetermine sample size. No data were excluded from the analyses. The experiments were not randomized. The investigators were not blinded to allocation during experiments and outcome assessment.

Reporting summary

Further information on research design is available in the Nature Portfolio Reporting Summary linked to this article.

Data availability

All data are available in the main text or the supplementary materials. RNA-seq data in this study have been deposited in the NCBI GEO database under BioProject ID PRJNA896729. All nitrifier genomes in this study were downloaded from the public NCBI RefSeq database (https://www.ncbi.nlm.nih.gov/refseq/). Source data are provided with this paper.

References

1. Kuypers, M. M., Marchant, H. K. & Kartal, B. The microbial nitrogen-cycling network. *Nat. Rev. Microbiol.* **16**, 263–276 (2018).
2. Konneke, M. et al. Isolation of an autotrophic ammonia-oxidizing marine archaeon. *Nature* **437**, 543–546 (2005).
3. Frankland, P. F. & Frankland, G. C. V. The nitrifying process and its specific ferment.—Part I. *Phil. Trans. R. Soc. B* **181**, 107–128 (1890).
4. Daims, H. et al. Complete nitrification by *Nitrospira* bacteria. *Nature* **528**, 504–509 (2015).
5. van Kessel, M. et al. Complete nitrification by a single microorganism. *Nature* **528**, 555–559 (2015).
6. Martens-Habbena, W., Berube, P. M., Urakawa, H., de la Torre, J. R. & Stahl, D. A. Ammonia oxidation kinetics determine niche separation of nitrifying Archaea and Bacteria. *Nature* **461**, 976–979 (2009).
7. Kits, K. D. et al. Kinetic analysis of a complete nitrifier reveals an oligotrophic lifestyle. *Nature* **549**, 269–272 (2017).
8. Jung, M.-Y. et al. Ammonia-oxidizing archaea possess a wide range of cellular ammonia affinities. *ISME J.* **16**, 272–283 (2022).
9. Li, P.-N. et al. Nutrient transport suggests an evolutionary basis for charged archaeal surface layer proteins. *ISME J.* **12**, 2389–2402 (2018).
10. Stahl, D. A. & de la Torre, J. R. Physiology and diversity of ammonia-oxidizing archaea. *Annu. Rev. Microbiol.* **66**, 83–101 (2012).
11. Monod, J. in *Selected Papers in Molecular Biology by Jacques Monod* (eds Lwoff A. & Ullman, A.) 139–162 (Academic Press, 2012).
12. Gorke, B. & Stulke, J. Carbon catabolite repression in bacteria: many ways to make the most out of nutrients. *Nat. Rev. Microbiol.* **6**, 613–624 (2008).
13. Fisher, S. H. & Sonenshein, A. L. Control of carbon and nitrogen metabolism in *Bacillus subtilis*. *Annu. Rev. Microbiol.* **45**, 107–135 (1991).
14. Beltran, G., Novo, M., Rozès, N., Mas, A. & Guillamón, J. M. Nitrogen catabolite repression in *Saccharomyces cerevisiae* during wine fermentations. *FEMS Yeast Res.* **4**, 625–632 (2004).
15. Bayer, B. et al. Physiological and genomic characterization of two novel marine thaumarchaeal strains indicates niche differentiation. *ISME J.* **10**, 1051–1063 (2016).
16. Tourna, M. et al. *Nitrososphaera viennensis*, an ammonia oxidizing archaeon from soil. *Proc. Natl Acad. Sci. USA* **108**, 8420–8425 (2011).
17. Urakawa, H. et al. *Nitrosospira lacus* sp. nov., a psychrotolerant, ammonia-oxidizing bacterium from sandy lake sediment. *Int. J. Syst. Evol. Microbiol.* **65**, 242–250 (2015).
18. Klotz, M. G. et al. Complete genome sequence of the marine, chemolithoautotrophic, ammonia-oxidizing bacterium *Nitrosococcus oceani* ATCC 19707. *Appl. Environ. Microbiol.* **72**, 6299–6315 (2006).
19. Koops, H. & Stehr, G. Classification of eight new species of ammonia-oxidizing bacteria: *Nitrosomonas communis* sp. nov., *Nitrosomonas ureae* sp. nov., *Nitrosomonas aestuarii* sp. nov., *Nitrosomonas marina* sp. nov., *Nitrosomonas nitrosa* sp. nov., *Nitrosomonas eutropha* sp. nov., *Nitrosomonas oligotropha* sp. nov. and *Nitrosomonas halophila* sp. nov. *Microbiology* **137**, 1689–1699 (1991).
20. Watson, S. W., Graham, L. B., Remsen, C. C. & Valois, F. W. A lobular, ammonia-oxidizing bacterium, *Nitrosolobus multiformis* nov. gen. nov. sp. *Arch. Mikrobiol.* **76**, 183–203 (1971).
21. Solomon, C. M., Collier, J. L., Berg, G. M. & Glibert, P. M. Role of urea in microbial metabolism in aquatic systems: a biochemical and molecular review. *Aquat. Microb. Ecol.* **59**, 67–88 (2010).
22. Berman, T. & Bronk, D. A. Dissolved organic nitrogen: a dynamic participant in aquatic ecosystems. *Aquat. Microb. Ecol.* **31**, 279–305 (2003).
23. Mobley, H. L. T., Island, M. D. & Hausinger, R. P. Molecular biology of microbial ureases. *Microbiol. Rev.* **59**, 451–480 (1995).
24. Kitzinger, K. et al. Cyanate and urea are substrates for nitrification by Thaumarchaeota in the marine environment. *Nat. Microbiol.* **4**, 234–243 (2019).
25. Qin, W. et al. Alternative strategies of nutrient acquisition and energy conservation map to the biogeography of marine ammonia-oxidizing archaea. *ISME J.* **14**, 2595–2609 (2020).
26. Sedlacek, C. J. et al. Transcriptomic response of *Nitrosomonas europaea* transitioned from ammonia- to oxygen-limited steady-state growth. *mSystems* **5**, e00562-19 (2020).
27. Stein, L. Y., Campbell, M. A. & Klotz, M. G. Energy-mediated vs. ammonium-regulated gene expression in the obligate ammonia-oxidizing bacterium, *Nitrosococcus oceani*. *Front. Microbiol.* **4**, 277 (2013).
28. Leigh, J. A. & Dodsworth, J. A. Nitrogen regulation in bacteria and archaea. *Annu. Rev. Microbiol.* **61**, 349–377 (2007).
29. Emori, M. T. et al. The deuridylylation activity of *Herbaspirillum seropedicae* GlnD protein is regulated by the glutamine: 2-oxoglutarate ratio. *Biochim. Biophys. Acta Proteins Proteom.* **1866**, 1216–1223 (2018).
30. Merrick, M. Post-translational modification of P_{II} signal transduction proteins. *Front. Microbiol.* **5**, 763 (2015).
31. Martens-Habbena, W. et al. The production of nitric oxide by marine ammonia-oxidizing archaea and inhibition of archaeal ammonia oxidation by a nitric oxide scavenger. *Environ. Microbiol.* **17**, 2261–2274 (2015).

32. Prosser, J. I. & Nicol, G. W. Archaeal and bacterial ammonia-oxidisers in soil: the quest for niche specialisation and differentiation. *Trends Microbiol.* **20**, 523–531 (2012).
33. Park, H. D., Wells, G. F., Bae, H., Criddle, C. S. & Francis, C. A. Occurrence of ammonia-oxidizing archaea in wastewater treatment plant bioreactors. *Appl. Environ. Microbiol.* **72**, 5643–5647 (2006).
34. Leininger, S. et al. Archaea predominate among ammonia-oxidizing prokaryotes in soils. *Nature* **442**, 806–809 (2006).
35. Alonso-Saez, L. et al. Role for urea in nitrification by polar marine Archaea. *Proc. Natl Acad. Sci. USA* **109**, 17989–17994 (2012).
36. Song, W. et al. Functional traits resolve mechanisms governing the assembly and distribution of nitrogen-cycling microbial communities in the global ocean. *mBio* **13**, e03832-21 (2022).
37. Mirandela, G. D., Tamburrino, G., Hoskisson, P. A., Zachariae, U. & Javelle, A. The lipid environment determines the activity of the *Escherichia coli* ammonium transporter AmtB. *FASEB J.* **33**, 1989–1999 (2019).
38. Wacker, T., Garcia-Celma, J. J., Lewe, P. & Andrade, S. L. A. Direct observation of electrogenic NH_4^+ transport in ammonium transport (Amt) proteins. *Proc. Natl Acad. Sci. USA* **111**, 9995–10000 (2014).
39. Williamson, G. et al. A two-lane mechanism for selective biological ammonium transport. *eLife* **9**, e57183 (2020).
40. Eppley, R. W., Rogers, J. N. & McCarthy, J. J. Half-saturation constants for uptake of nitrate and ammonium by marine phytoplankton. *Limnol. Oceanogr.* **14**, 912–920 (1969).
41. Kirchman, D. L. The uptake of inorganic nutrients by heterotrophic bacteria. *Microb. Ecol.* **28**, 255–271 (1994).
42. Button, D. Nutrient uptake by microorganisms according to kinetic parameters from theory as related to cytoarchitecture. *Microbiol. Mol. Biol. Rev.* **62**, 636–645 (1998).
43. Button, D. & Robertson, B. Effect of nutrient kinetics and cytoarchitecture on bacterioplankter size. *Limnol. Oceanogr.* **45**, 499–505 (2000).
44. Lehtovirta-Morley, L. E. et al. Isolation of '*Candidatus* Nitrosocosmicus franklandus', a novel ureolytic soil archaeal ammonia oxidiser with tolerance to high ammonia concentration. *FEMS Microbiol. Ecol.* **92**, fiw057 (2016).
45. Koch, H., van Kessel, M. A. H. J. & Lücker, S. Complete nitrification: insights into the ecophysiology of comammox *Nitrospira*. *Appl. Microbiol. Biotechnol.* **103**, 177–189 (2019).
46. Qin, W. et al. *Nitrosopumilus maritimus* gen. nov., sp. nov., *Nitrosopumilus cobalaminigenes* sp. nov., *Nitrosopumilus oxyclinae* sp. nov., and *Nitrosopumilus ureiphilus* sp. nov., four marine ammonia-oxidizing archaea of the phylum Thaumarchaeota. *Int. J. Syst. Evol. Microbiol.* **67**, 5067–5079 (2017).
47. Stieglmeier, M. et al. *Nitrososphaera viennensis* gen. nov., sp. nov., an aerobic and mesophilic, ammonia-oxidizing archaeon from soil and a member of the archaeal phylum Thaumarchaeota. *Int. J. Syst. Evol. Microbiol.* **64**, 2738–2752 (2014).
48. Lunau, M., Lemke, A., Walther, K., Martens-Habbena, W. & Simon, M. An improved method for counting bacteria from sediments and turbid environments by epifluorescence microscopy. *Environ. Microbiol.* **7**, 961–968 (2005).
49. Holmes, R. M., Aminot, A., Kérouel, R., Hooker, B. A. & Peterson, B. J. A simple and precise method for measuring ammonium in marine and freshwater ecosystems. *Can. J. Fish. Aquat. Sci.* **56**, 1801–1808 (1999).
50. García-Robledo, E., Corzo, A. & Papaspyrou, S. A fast and direct spectrophotometric method for the sequential determination of nitrate and nitrite at low concentrations in small volumes. *Mar. Chem.* **162**, 30–36 (2014).
51. Fawcett, J. K. & Scott, J. E. A rapid and precise method for the determination of urea. *J. Clin. Pathol.* **13**, 156–159 (1960).
52. McIlvin, M. R. & Altabet, M. A. Chemical conversion of nitrate and nitrite to nitrous oxide for nitrogen and oxygen isotopic analysis in freshwater and seawater. *Anal. Chem.* **77**, 5589–5595 (2005).
53. Sigman, D. M. et al. A bacterial method for the nitrogen isotopic analysis of nitrate in seawater and freshwater. *Anal. Chem.* **73**, 4145–4153 (2001).
54. Weigand, M. A., Foriel, J., Barnett, B., Oleynik, S. & Sigman, D. M. Updates to instrumentation and protocols for isotopic analysis of nitrate by the denitrifier method. *Rapid Commun. Mass Spectrom.* **30**, 1365–1383 (2016).
55. Zhang, L., Altabet, M. A., Wu, T. & Hadas, O. Sensitive measurement of $NH_4^{+\,15}N/^{14}N$ ($\delta^{15}NH_4^+$) at natural abundance levels in fresh and saltwaters. *Anal. Chem.* **79**, 5297–5303 (2007).
56. Peng, X. et al. Long-term fertilization alters the relative importance of nitrate reduction pathways in salt marsh sediments. *J. Geophys. Res. Biogeosci.* **121**, 2082–2095 (2016).
57. Granger, J. & Sigman, D. M. Removal of nitrite with sulfamic acid for nitrate N and O isotope analysis with the denitrifier method. *Rapid Commun. Mass Spectrom.* **23**, 3753–3762 (2009).
58. Pett-Ridge, J. & Weber, P. K. in *Microbial Systems Biology: Methods and Protocols* (ed. Navid, A.) 91–136 (Springer, 2022).
59. Dekas, A. E. et al. Characterizing chemoautotrophy and heterotrophy in marine archaea and bacteria with single-cell multi-isotope nanoSIP. *Front. Microbiol.* **10**, 2682 (2019).
60. Martens-Habbena, W. & Stahl, D. A. in *Methods in Enzymology* Vol. 496 (eds Klotz, M. G. & Stein, L. Y.) 465–487 (Academic Press, 2011).
61. Simon, M. & Azam, F. Protein content and protein synthesis rates of planktonic marine bacteria. *Mar. Ecol. Prog. Ser.* **51**, 201–213 (1989).
62. Qin, W. et al. Stress response of a marine ammonia-oxidizing archaeon informs physiological status of environmental populations. *ISME J.* **12**, 508–519 (2018).
63. Bolger, A. M., Lohse, M. & Usadel, B. Trimmomatic: a flexible trimmer for Illumina sequence data. *Bioinformatics* **30**, 2114–2120 (2014).
64. Langmead, B. & Salzberg, S. L. Fast gapped-read alignment with Bowtie 2. *Nat. Methods* **9**, 357–359 (2012).
65. Danecek, P. et al. Twelve years of SAMtools and BCFtools. *GigaScience* **10**, giab008 (2021).
66. Putri, G. H., Anders, S., Pyl, P. T., Pimanda, J. E. & Zanini, F. Analysing high-throughput sequencing data in Python with HTSeq 2.0. *Bioinformatics* **38**, 2943–2945 (2022).
67. Love, M. I., Huber, W. & Anders, S. Moderated estimation of fold change and dispersion for RNA-seq data with DESeq2. *Genome Biol.* **15**, 550 (2014).
68. Bowers, R. M. et al. Minimum information about a single amplified genome (MISAG) and a metagenome-assembled genome (MIMAG) of bacteria and archaea. *Nat. Biotechnol.* **35**, 725–731 (2017).
69. Almeida, A. et al. A unified catalog of 204,938 reference genomes from the human gut microbiome. *Nat. Biotechnol.* **39**, 105–114 (2021).
70. Buchfink, B., Reuter, K. & Drost, H.-G. Sensitive protein alignments at tree-of-life scale using DIAMOND. *Nat. Methods* **18**, 366–368 (2021).
71. Parks, D. H., Imelfort, M., Skennerton, C. T., Hugenholtz, P. & Tyson, G. W. CheckM: assessing the quality of microbial genomes recovered from isolates, single cells, and metagenomes. *Genome Res.* **25**, 1043–1055 (2015).
72. Teufel, F. et al. SignalP 6.0 predicts all five types of signal peptides using protein language models. *Nat. Biotechnol.* **40**, 1023–1025 (2022).

73. Parks, D. H. et al. A complete domain-to-species taxonomy for Bacteria and Archaea. *Nat. Biotechnol.* **38**, 1079–1086 (2020).
74. Chaumeil, P.-A., Mussig, A. J., Hugenholtz, P. & Parks, D. H. GTDB-Tk v2: memory friendly classification with the genome taxonomy database. *Bioinformatics* **38**, 5315–5316 (2022).
75. Minh, B. Q. et al. IQ-TREE 2: new models and efficient methods for phylogenetic inference in the genomic era. *Mol. Biol. Evol.* **37**, 1530–1534 (2020).

Acknowledgements

We thank Z. Perry, B. Quan and T. Tubbs for technical assistance in growth experiments and S. Oleynik for maintaining the mass spectrometer for stable isotope analysis. *N. inopinata* was generously provided by H. Daims, University of Vienna. *N. piranensis* was generously provided by A. Santoro and B. Bayer, University of California, Santa Barbara. *N. multiformis* was kindly provided by J. Norton, Utah State University. *N. ureae* was kindly provided by A. Pommerening-Röser, University of Hamburg. This work was supported by National Natural Science Foundation of China grants 42277304 and 41977056 (to B.W.) and 42276117 (Y. Zheng). This work was also supported by the startup funding of the University of Oklahoma (to W.Q.). Work was also funded by the US Department of Energy's Office of Science, Division of Biological and Environmental Research Program (Grant DE-SC0020356 to M.-K.H.W., X.M., D.A.S., C.P., Z.F., B.A. and S.P.W.) and by the Defense Advanced Research Projects Agency (Contract Number HR0011-17-2-0064 to M.-K.H.W., D.A.S. and S.P.W.). Funding was also provided by Florida Agricultural Experiment Station Hatch project FLA-FTL-005680, UF IFAS Early Career Award and USDA NIFA award number 2022-67019-36501 (to W.M.-H.). Part of this work was performed at the Lawrence Livermore National Laboratory under Contract DE-AC52-07NA27344. The participation of X.W. and B.B.W. was supported by Simons Foundation grant 675459 to B.B.W. X.S. was supported by a G. Evelyn Hutchinson postdoctoral fellowship from Yale Institute for Biospheric Studies at Yale University. H.U. was supported by National Science Foundation grant DEB-1664052.

Author contributions

W.Q., D.A.S., B.B.W., X.M., W.M.-H. and M.-K.H.W. designed the experiments. W.Q., S.P.W., Y. Zheng, E.C., X.L., J. Johnston, X.W., B.A. and Z.F. performed the experiments and analysed data with input from B.W., H.L., L.H., Q.T., W.W.C., X.S., M.W., L.N., K.A.H., H.U., X.T., Dongyu Wang, X.Y., Dazhi Wang, C.P., P.K.W., J. Jiang, Y. Zhang and J.Z. W.Q., S.P.W., D.A.S., W.M.-H. and M.-K.H.W. wrote the paper, with contributions and approval from all other authors.

Competing interests

The authors declare no competing interests.

Additional information

Extended data is available for this paper at https://doi.org/10.1038/s41564-023-01593-7.

Supplementary information The online version contains supplementary material available at https://doi.org/10.1038/s41564-023-01593-7.

Correspondence and requests for materials should be addressed to Wei Qin, Willm Martens-Habbena or Mari-Karoliina H. Winkler.

Peer review information *Nature Microbiology* thanks Marc Strous and the other, anonymous, reviewer(s) for their contribution to the peer review of this work.

Reprints and permissions information is available at www.nature.com/reprints.

Publisher's note Springer Nature remains neutral with regard to jurisdictional claims in published maps and institutional affiliations.

[1]School of Biological Sciences, Institute for Environmental Genomics, University of Oklahoma, Norman, OK, USA. [2]Department of Civil and Environmental Engineering, University of Washington, Seattle, WA, USA. [3]State Key Laboratory of Marine Environmental Science, College of the Environment and Ecology, Xiamen University, Xiamen, Fujian, China. [4]Department of Microbiology and Cell Science, Fort Lauderdale Research and Education Center, University of Florida, Davie, FL, USA. [5]Lawrence Livermore National Laboratory, Livermore, CA, USA. [6]Department of Geosciences, Princeton University, Princeton, NJ, USA. [7]College of Life Sciences, Nanjing Agricultural University, Nanjing, Jiangsu, China. [8]Department of Ecology and Evolutionary Biology, Yale University, New Haven, CT, USA. [9]Department of Ecology and Environmental Studies, Florida Gulf Coast University, Fort Myers, FL, USA. [10]State Key Laboratory of Soil and Sustainable Agriculture, Institute of Soil Science, Chinese Academy of Sciences, Nanjing, China. [11]State Key Laboratory of Marine Environmental Science, College of Ocean and Earth Sciences, Xiamen University, Xiamen, Fujian, China. [12]These authors contributed equally: Wei Qin, Stephany P. Wei, Yue Zheng, Eunkyung Choi. ✉e-mail: weiqin@ou.edu; w.martenshabbena@ufl.edu; mwinkler@uw.edu